APL Materials

Analysis of the temperature dependence of the thermal conductivity of insulating single crystal oxides

Cite as: APL Mater. 4, 104815 (2016); https://doi.org/10.1063/1.4966220
Submitted: 03 August 2016 • Accepted: 07 October 2016 • Published Online: 31 October 2016

E. Langenberg, E. Ferreiro-Vila, V. Leborán, et al.

Analysis of the temperature dependence of the thermal conductivity of insulating single crystal oxides

E. Langenberg,[1] E. Ferreiro-Vila,[1] V. Leborán,[1] A. O. Fumega,[2] V. Pardo,[2] and F. Rivadulla[1,a]

[1]*Centro de Investigación en Química Biolóxica e Materiais Moleculares (CIQUS) and Departamento de Química-Física, Universidade de Santiago de Compostela, 15782 Santiago de Compostela, Spain*

[2]*Departamento de Física Aplicada, Universidade de Santiago de Compostela, 15782 Santiago de Compostela, Spain*

(Received 3 August 2016; accepted 7 October 2016; published online 31 October 2016)

The temperature dependence of the thermal conductivity of 27 different single crystal oxides is reported from ≈20 K to 350 K. These crystals have been selected among the most common substrates for growing epitaxial thin-film oxides, spanning over a range of lattice parameters from ≈3.7 Å to ≈12.5 Å. Different contributions to the phonon relaxation time are discussed on the basis of the Debye model. This work provides a database for the selection of appropriate substrates for thin-film growth according to their desired thermal properties, for applications in which heat management is important. [http://dx.doi.org/10.1063/1.4966220]

The application of epitaxial thin films to a broad range of phenomena which require a detailed knowledge of heat transport (thermoelectricity, heat-assisted spin-transfer effects, thermal insulation and heat dissipation in nanostructures, etc.) is becoming increasingly important. In this case, the ability of electrically insulating substrates to conduct heat makes the analysis of the thermal conductivity of thin films far more complicated than that of the electrical conductivity.[1,2] For the particular case of oxides, strain engineering by epitaxial growth of thin films is a powerful technique when it comes to gaining access to novel phases, and thus engineering new or enhanced functional properties.[3] A systematic variation of the film properties requires therefore the use of different substrates, which may differ substantially in their lattice parameters and orientation. As a result, different crystalline substrates should be selected not only according to the lattice mismatch with the film, but also depending on its thermal properties, at least for some specific applications (i.e., nanostructured thermoelectrics, thermal-induced spin-related phenomena, phononics, etc.).

Here we report the temperature dependence of the thermal conductivity of a large variety of single crystal oxides, covering the range of lattice parameters used to grow the vast majority of epitaxial thin films. A detailed analysis on the basis of the Debye model[2] suggests an important role for defect-scattering events, even in high quality single crystals. This produces very large variations of the thermal conductivity among crystals of the same family (perovskites, for instance) in spite of their similar Debye temperatures, Θ_D.

The cross-plane thermal conductivity of 27 different single-crystal oxides was measured by the 3ω-method[4,5] (see the supplementary material for details). The crystals were obtained from Crystec GmbH (http://www.crystec.de). They are one-side mirror-polished $5 \times 5 \times 0.5$ mm single crystals and were measured as received. The range of lattice parameters explored is schematically shown in Figure 1. The actual compositions analyzed and the experimental values of κ(T) between 20 K and 350 K are available in the supplementary material (Tables AI-IV).

[a]Author to whom correspondence should be addressed. Electronic mail: f.rivadulla@usc.es

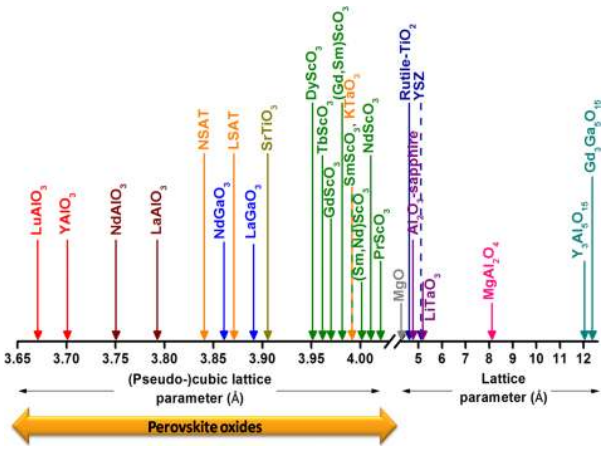

FIG. 1. Pseudocubic lattice parameter of the different oxides studied in this work. The line covers the range from a = 3.67 Å of $LuAlO_3$ to the 12.4 Å of $Gd_3Ga_5O_{12}$. See the supplementary material for the different compositions of $REScO_3$ studied in this work.

At low temperatures, typically below 100 K, the rapid increase of the thermal conductivity increases the thermal diffusion length, which approaches the physical thickness of the crystal and establishes a limit for the applicability of the 3ω method. This is particularly important for the samples with higher thermal conductivity. At low frequencies, the in-phase $V_{3\omega}$ decays logarithmically, defining a linear regime in a $V_{3\omega}$ *vs.* log(2ω) plot, and a constant out-of-phase component. Given the difficulties to calculate accurately the thermal diffusivities, we limited our analysis to this linear regime, optimizing the dissipated power through the resistor accordingly (see Figure S1 in the supplementary material for further details about acquisition and analysis of the data).

Also, the decrease of the characteristic dR/dT of the heater below 40 K introduces an extra source of error at low temperatures (see Figure S1).

For all these reasons, the error of κ at the lowest temperatures (<40 K) increases, particularly in the samples with very large thermal conductivity at low temperatures.

Additionally, some crystals of $SrTiO_3$ were treated in order to obtain a TiO_2-terminated surface, according to Ref. 6. We have found no difference in the thermal conductivity with respect to "as received" crystals.

The temperature dependence of the thermal conductivity, κ(T), is shown in Figure 2 for 16 different oxides, representative of the variety of behaviors observed in the different families of crystalline structures and compositions discussed in this work.

For most of these oxides κ(T) is in agreement with the expectations for a crystalline system in which phonon-phonon *Umklapp* scattering dominates at high temperatures, plus a boundary scattering term which limits the phonon-propagation at low temperatures.[7]

Still, we have observed important departures from this behavior in some systems: $(NdAlO_3)_{0.39}$–$(SrAl_{0.5}Ta_{0.5}O_3)_{0.61}$ (NSAT), $(LaAlO_3)_{0.29}$–$(SrAl_{0.5}Ta_{0.5}O_3)_{0.71}$ (LSAT), and Yttria-stabilized zirconia (9.5%-Y_2O_3:ZrO_2, YSZ) show a very large reduction of κ(T) with respect to $SrTiO_3$ and other perovskites with similar lattice parameters, structure, and density (see Figures 2(b) and 2(f)). This is a consequence of the effect of random cationic substitution, which has an enormous impact on the lattice dynamics.[8–10]

More surprising is however the low value and temperature dependence of the thermal conductivity in the family of rare-earth scandates (Figure 2(d)). In this case, κ(T) is largely suppressed with respect to its expected value in the whole temperature range, in spite of their excellent crystalline quality. A large reduction was also observed in κ(T) of the ferroelectric oxide $LiTaO_3$ with regard to other incipient ferroelectric materials like $KTaO_3$ and $SrTiO_3$ (Figure 2(e)).

The Debye temperature, Θ_D, defines the characteristic energy scale of the crystal lattice, and determines the intrinsic mechanisms of phonon dispersion in the material. At temperatures not too far

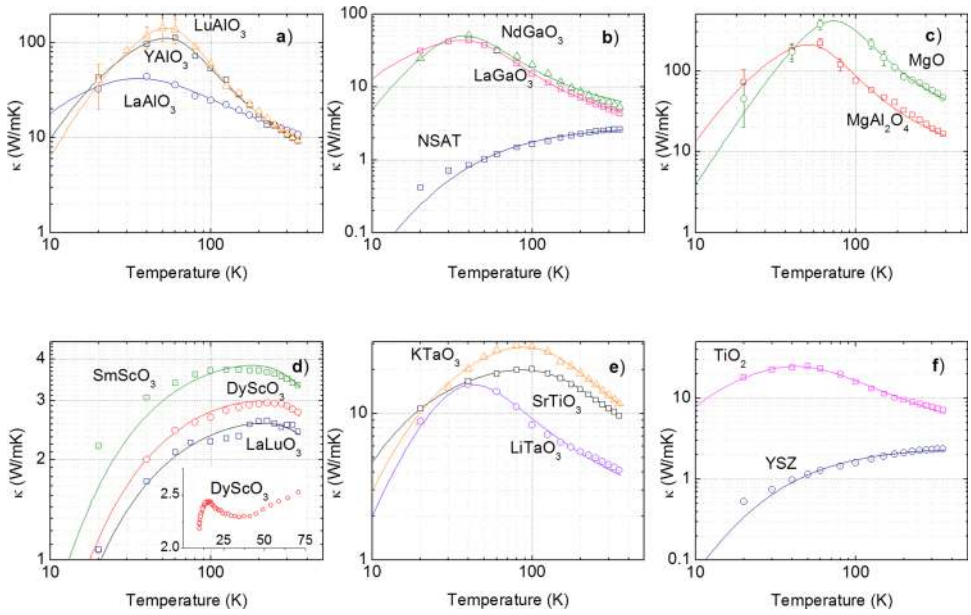

FIG. 2. Log-log plot of the temperature dependence of κ(T) for some representative oxides studied in this work. The solid lines over the experimental points represent the fittings to the Debye model (see the discussion in the text). Panels (a) and (b) show κ(T) for different perovskites. The behavior of rock-salt MgO and cubic spinel $MgAl_2O_4$ is compared in (c). (d) κ(T) for rare-earth perovskite scandates and $LaLuO_3$. The inset shows a detailed low temperature measurement for $DyScO_3$. (e) Comparison of κ(T) in ferroelectric $LiTaO_3$ with incipient-ferroelectric $KTaO_3$ and $SrTiO_3$. (f) Comparison of κ(T) in TiO_2-rutile and YSZ.

away from Θ_D, anharmonic phonon-phonon *Umklapp* scattering is the main mechanism responsible for the intrinsic value and temperature dependence of κ(T), which can be approximated by,[2]

$$\kappa = \xi \frac{\overline{M}\delta\Theta_D^3}{\gamma^2 T n^{2/3}}. \tag{1}$$

$\overline{M}$ is the average molar mass per atom in a crystal with n atoms per formula unit (Z molecules per unit cell), $\delta = \left(\frac{V}{nZ}\right)^{1/3}$ is the cubic root of the volume per atom, γ is the Grüneissen factor and ξ is a constant which can be calculated according to

$$\xi = \left\{ \frac{2.43 \times 10^{-8}}{\left(1 - \frac{0.514}{\gamma} + \frac{0.228}{\gamma^2}\right)} \right\}. \tag{2}$$

An estimation of κ in this temperature range can be made if the actual values of Θ_D and γ can be measured or calculated for each material. For some of the oxides treated in this work, values of γ ≈ 1-1.5 are reported in the literature from the thermal expansion and specific heat data.[11–13] However, these are average values including the contribution from optical modes with a very small dispersion. For an appropriate estimation of κ according to Equation (1), the value of γ from predominant acoustic modes close to Θ_D, the main heat carriers at these temperatures, is needed. Unfortunately, these are unavailable for most materials, and therefore γ will be used as an adjustable parameter, the only free fitting parameter in Equation (1) for a comparison with our experimental thermal conductivity data. Although Equation (1) cannot be trusted for quantitative calculations of the thermal conductivity, it should predict correctly the trends of the experimental thermal conductivity with the Debye temperature, mass density, etc.

On the other hand, Θ_D can be calculated from its proportionality to the average sound velocity,

$$\Theta_D = \frac{h v_m}{k_B}\left[\frac{3n}{4\pi}\left(\frac{N_A \rho}{M}\right)\right]^{1/3}, \tag{3}$$

where ρ denotes the density, v_m the average speed of sound, and M the molar mass. If we now approximate these oxides to elastically isotropic crystals, v_m can be calculated from the bulk and shear modulus, B and G, through the averaged longitudinal and transverse components of the phonon velocity,

$$v_m = \left[\frac{1}{3}\left(\frac{2}{v_t^3} + \frac{1}{v_l^3}\right)\right]^{-1/3}, \tag{4}$$

$$v_t = \sqrt{\frac{G}{\rho}},\ v_l = \sqrt{\frac{B + \left(\frac{4}{3}G\right)}{\rho}}. \tag{5}$$

Anderson[14] worked out the relationship between B and G, and the stiffness constants c_{ij} of the elastic tensor,

$$B = \frac{1}{9}(c_{11} + c_{22} + c_{33}) + \frac{2}{9}(c_{12} + c_{13} + c_{23}),$$
$$G = \frac{1}{15}(c_{11} + c_{22} + c_{33}) - \frac{1}{15}(c_{12} + c_{13} + c_{23}) + \frac{1}{5}(c_{44} + c_{55} + c_{66}). \tag{6}$$

The values of these constants can be either measured experimentally, for example, through resonant ultrasound spectroscopy (RUS), or calculated *ab initio*. For $DyScO_3$, $GdScO_3$, $NdScO_3$, and $SmScO_3$ we calculated the values of v_m from the experimental RUS data available in the literature.[15–17] For $TbScO_3$, $PrScO_3$ and mixed compositions (Sm,Gd and Sm,Nd), v_m was estimated from the interpolation of the v_m *vs*. tolerance factor (or density) for the other four $REScO_3$ oxides.

Experimental or calculated values of the stiffness constants were used to obtain v_m for the majority of oxides treated in this work.[18–25]

The values calculated for the average sound velocity following this procedure are shown in Figure 3(a), as a function of the mass density, and listed in Tables BI-IV in the supplementary material.

The average sound velocity shows a continuous reduction as density increases (Figure 3(a)). Birch[26] and other authors,[21] observed that the average sound velocity increases with pressure, i.e.,v_m increases when the volume decreases at constant atomic mass. However, v_m decreases on increasing density along a series in which the atomic mass is not constant.[21] In oxides, most of the volume is occupied by the oxygen sublattice, and for the particular set of materials studied in this work the volume per atom (δ in tables B-I to B-IV in the supplementary material) is very similar. Therefore, the decrease of v_m with density is in agreement with the variation of the mean atomic mass, observed in Figure 3(b).

The dashed line in Figure 3(a) represents the expected behavior for a B = 200 GPa, which is the value for most perovskite oxides,[27,28] as well as for $Y_3Al_5O_{12}$ (YIG) and $Gd_3Ga_5O_{12}$ (GGG) garnets.[29] The trends observed in this plot and the agreement with the expectations for B = 200 GPa supports the validity and accuracy of our calculations for v_m.

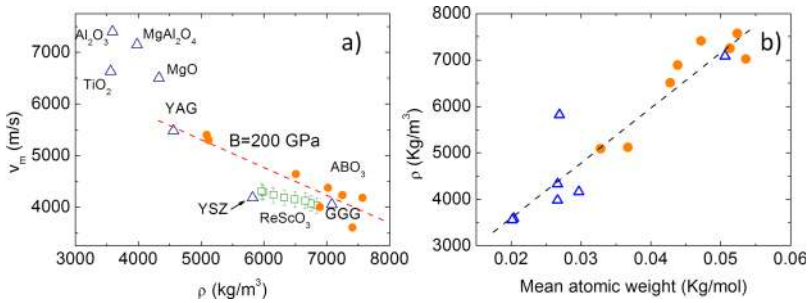

FIG. 3. (a) Average sound velocity calculated from Equations (4)–(6), as a function of the mass density. (b) Mass density as a function of the molecular weight per atom. Open triangles, open squares, and closed circles represent the values for non-perovskites, rare-earth Sc perovskites, and other perovskites, respectively.

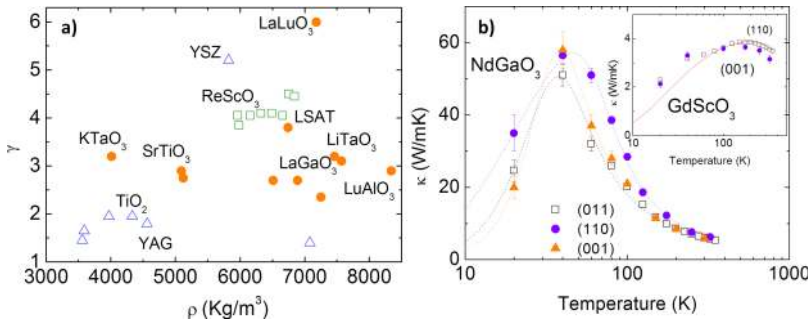

FIG. 4. (a) The values of γ that best fit the experimental κ at $T = \Theta_D/2$, as a function of density. Open triangles, open squares, and closed circles represent the values for non-perovskites, rare-earth Sc perovskites, and other perovskites, respectively. (b) κ(T) of orthorhombic $NdGaO_3$ and $GdScO_3$ (inset) along different crystallographic directions.

The values of Θ_D were calculated from v_m for each oxide, and are listed in Tables B-I to B-IV (supplementary material). We double-checked our results by comparison with experimental values of Θ_D from specific heat, when available, obtaining a satisfactory agreement. From Θ_D we calculated the thermal conductivity at $T = (\Theta_D/2)$ for each material, according to Equation (1), using the Grüneissen parameter, γ, as the only fitting parameter (Figure 4(a)). The values of γ used for a satisfactory agreement between the observed and calculated $\kappa(\Theta_D/2)$ are shown in Figure 3(d) for all oxides. The actual results are also listed in Tables B-I to B-IV in the supplementary material.

The values of γ from these fittings range between ≈1.3 and 2 for garnets, rock-salt MgO, rutile TiO_2, and other low-density non-perovskite materials (open triangles in Figure 3(c)). This is in good agreement with previous reports from experimental thermal expansion data: White and Anderson calculated a γ = 1.5-1.6 for MgO,[11] which compares very satisfactorily with our γ ≈ 1.45; similar experiments for $MgAl_2O_4$ gave γ = 1.4,[30] also close to the value of γ ≈ 1.65 from our fittings.

Therefore, we conclude that in these non-perovskite oxides the thermal conductivity is determined by Umklapp phonon-phonon scattering at temperatures not too far from their Debye temperature.

On the other hand, γ increases up to ≈2.5-3 for perovskites and reaches the value of γ ≈ 4-4.5 for LSAT and $REScO_3$. Crystalline anisotropy has a negligible effect on these results. The thermal conductivity shows only a small anisotropy in orthorhombic stoichiometric crystals like $NdGaO_3$, particularly at low temperatures (Figure 4(b)). The effect is even smaller in $REScO_3$.

These observations indicate that factors other than purely phonon-phonon scattering (boundary, isotope, vacancy, or impurity scattering) cannot be neglected already in this temperature range.

Therefore, in order to understand which processes govern κ(T) in this wide range of oxides, we fitted the experimental data to the Debye model in the whole temperature range. Assuming a linear dispersion relation for acoustic phonons, the general expression for the thermal conductivity in the relaxation time approximation is as follows:[7,31]

$$\kappa(T) = \frac{1}{2v\pi^2}\int_0^{\omega_D} \tau(\omega)\frac{\hbar\omega^4}{k_B T^2}\frac{e^{\frac{\hbar\omega}{k_B T}}}{\left(e^{\frac{\hbar\omega}{k_B T}}-1\right)^2}d\omega, \tag{7}$$

where ω is the phonon frequency (ω_D is the Debye frequency), and the relaxation time τ(ω) is the sum of the contribution of different processes to the thermal resistivity,

$$\tau^{-1}(\omega) = A + B\omega^2 T e^{\left(\frac{-\Theta_D}{\alpha T}\right)} + C\omega^4 = \frac{v_m}{\phi} + \frac{\hbar\gamma^4}{\overline{M}v^2\Theta_D}\omega^2 T e^{\left(\frac{-\Theta_D}{\alpha T}\right)} + \frac{\delta^3}{4\pi v_m^3}\sum_{i=1}^{N} x_i\left(1-\frac{\Delta M_i}{\overline{M}}\right)^2\omega^4. \tag{8}$$

The first term represents the domain boundary scattering: ϕ in the expression for A is related to the grain boundaries in polycrystalline materials, or the diameter of an effective cross-sectional area in the case of a single crystal; the second term represents the Umklapp processes, which enters

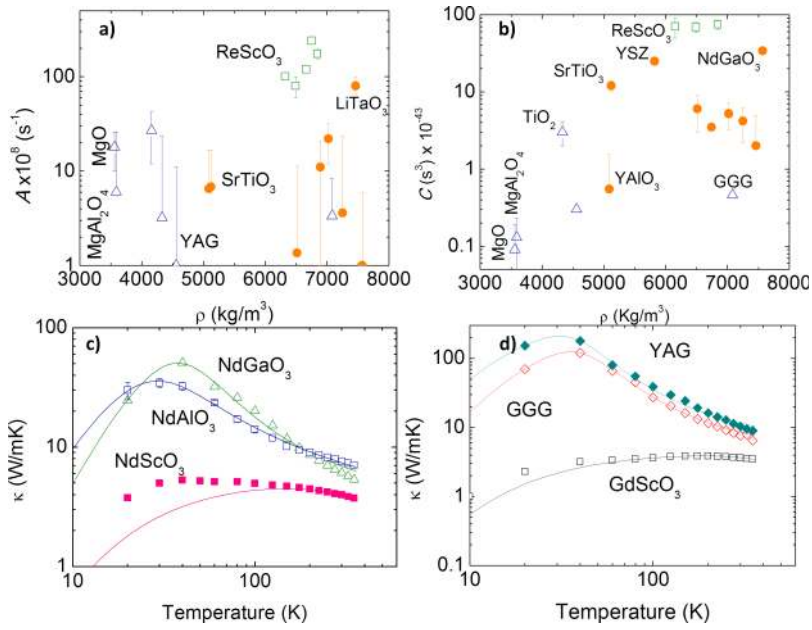

FIG. 5. The boundary scattering parameter A (a), and the impurity scattering term C (b) in Equation (8), derived from the fittings of experimental κ(T) to Equation (7). Open triangles, open squares, and closed circles represent the values for non-perovskites, rare-earth scandium perovskites, and other perovskites, respectively. (c) κ(T) of $NdBO_3$ (B = Ga, Al and Sc) perovskites. (d) Comparison of the thermal conductivities of $GdScO_3$ perovskite and $Y_3Al_5O_{12}$ (YAG), $Gd_3Ga_5O_{12}$ (GGG) garnets. Solid lines represent the best fitting to Equation (7).

into Equation (8) with a very similar expression to Equation (1). To minimize the number of free parameters and to improve the accuracy and meaning of the fittings, the values of v_m and Θ_D obtained before were used in Equation (8). Using these parameters, B is in the range of $\approx 10^{-18}$ -10^{-19} s/K for all the oxides in this work. The factor α is an adjustable parameter in the exponential term, which we kept always between 2 and 3, as in Ref. 9. The third term in Equation (8) is due to Rayleigh-like scattering by point-defects, including impurities, vacancies, and isotopes. In the expression for C, we have considered the effect of mass difference, ΔM_i, between the different impurities (with the molar fraction x_i) and the host atom. Other effects like volume changes and variations in the force constant of bonds might also be very important and should be included as extra terms in C. However, for the sake of simplicity and given the lack of accurate information about these factors, we included their effect as an effective value of C.

Best fits of κ(T) to Equation (7) are shown as solid lines in Figure 2. The parameter B was only varied slightly from its calculated value, for example, $B \approx 10^{-18}$ sK^{-1} for the perovskites assuming an average $\gamma = 2$.

The values of the domain boundary scattering parameter A (Figure 5(a)) are consistent with several micron-size domains, after using the corresponding phonon velocities. Again the case of $RESCO_3$ and other defective crystals like YSZ deviates from this behavior. It is also worth remarking the significantly larger value of the domain boundary parameter in $LiTaO_3$ (corresponding to domain sizes ≈700 nm) than in $SrTiO_3$ and $KTaO_3$. Whereas $LiTaO_3$ is ferroelectric, $SrTiO_3$ and $KTaO_3$ are not ferroelectric, although they show incipient ferroelectric character.[32–34] Ferroelectric domain walls have been shown to be a source of phonon scattering, reducing the thermal conductivity.[35,36] Therefore, although the values of A must be taken carefully because of the increasing inaccuracy in the determination of the lowest temperature κ(T), the observed trend could indeed suggest an effect of ferroelectric domain-boundary scattering in $LiTaO_3$.

On the other hand, fitting of the experimental data for most of the non-perovskites, like YAG, MgO, $MgAl_2O_4$, and Al_2O_3, give values of $C \approx 10^{-44}$ s^3 (see Figure 5(b)). The effect of isotope

scattering can be calculated on the basis of the natural abundance and mass difference of the isotopes,[9] giving $C \approx 10^{-44}$ s^3 for most of these oxides. This defines an excellent quality and negligible impurity content in most non-perovskite crystals.

However, isotope scattering cannot justify the values of $C \approx 10^{-42}$ s^3 observed in $LaGaO_3$ and $SrTiO_3$, and particularly, the very large values of $C \approx 5 \times 10^{-41}$ s^3 in $REScO_3$ and $LaLuO_3$.

Atomic substitutions and oxygen vacancies are relatively frequent in many 3*d* perovskite oxides. In the case of a vacancy, the mass difference with respect to the host atom is maximum (100%), and therefore even small concentrations cause a sizable reduction of the thermal conductivity.[37] Assuming ≈3%-4% of oxygen vacancies in $LaGaO_3$ produce $C \approx 10^{-42}$ s^3. For the case of $SrTiO_3$, the concentration of oxygen vacancies that would be required to justify the impurity scattering parameter is ≈10% according to our model. These numbers are probably slightly overestimated, as we did not consider explicitly the effect of the variation in volume and force constant associated to the vacancies or the possibility of cationic vacancies in addition to the oxygen. In any case, they are within the realistic number of defects observed in many of these perovskites.

On the other hand, the large value of C in $REScO_3$ needs further discussion, as there are many possible sources of phonon scattering which could reduce their thermal conductivity. *A priori*, the most important comes from the magnetic moment of the RE ions. Ke *et al.*[38] reported a magnetic phase transition at 3.1 K in $DyScO_3$, towards a low temperature antiferromagnetic phase induced by dipolar interaction among the Dy^{3+} ions. This is indeed observed as a slight increase of the magnetization around 15 K in the thermal conductivity (see the inset to Figure 2(d)).

Also, the crystal field environment of the perovskite splits the atomic 4f states of the small RE^{3+} ions, resulting in a ground-state with multiple electronic levels. A phonon with the correct energy to induce a transition between two of these states can be absorbed and later reemitted in a resonant scattering process which contributes to the thermal resistivity.[39,40] The effectiveness of this scattering mechanism will depend on the RE^{3+}-cross section and overall on the existence of electronic levels within the ground state manifold with the correct spacing to absorb a phonon.

Assuming a pseudocubic isotropic lattice, the energy of transverse and longitudinal acoustic phonons at the boundary of the Brillouin zone can be estimated from their respective velocities.[41] For $REScO_3$, we calculated an average value of ≈250 cm^{-1} (≈350 K). Above this energy (or temperature), resonant scattering of phonons by magnetic impurities will not contribute substantially to the thermal resistivity.

We have performed *ab initio* calculations based on the density functional theory[42] using the WIEN2k code[43] to obtain the electronic structure of various configurations of Nd^{3+}:4f states in $NdScO_3$[44] and $NdGaO_3$[45] (LDA + U,[46] with U = 8 eV, J = 1 eV). We have been able to obtain the solution for the ground state and two of the excited states for each oxide. These correspond to an energy difference ≈362-377 cm^{-1} and 746-774 cm^{-1} with respect to the ground state, too large to contribute to the resonant scattering. Moreover, the position of the excited levels in $NdScO_3$ and $NdGaO_3$ is very similar. Given that κ(T) of $NdScO_3$ is an order of magnitude smaller that $NdGaO_3$ or $NdAlO_3$ (see Figure 5(c)), our data suggest that resonant magnetic scattering is not responsible for the large suppression of the thermal conductivity in $REScO_3$.

Other observations give further support to this hypothesis:

(i) Gd^{3+} is a $4f^7$ ion with a large splitting between the ground and first excited states (>>350 K). Therefore, the magnetic resonant-scattering mechanism will not contribute to the thermal resistivity. This assumption is corroborated by the very similar κ(T) of Gd-Ga and Y-Ga garnets (Figure 5(d)). However, the thermal conductivity of $GdScO_3$ is largely suppressed with respect to calculations from the Debye model.

(ii) Lu^{3+} is a closed shell $4f^{14}$ rare earth ion, and therefore the resonant magnetic scattering is irrelevant. However, orthorhombic $LaLuO_3$ shows a very similar κ(T) to the scandates (Figure 2(d)). This calls for the existence of a similar (non-magnetic) origin for the low thermal conductivity of $REScO_3$ and $LaLuO_3$.

X-ray and chemical composition analysis by different groups confirmed that the true composition of these crystals is actually closer to $(La_{0.95}Lu_{0.05})LuO_3$ and $RE_{0.95}\ ScO_{2.95}$.[47–51] Considering that ≈4%-5% of Lu^{+3} occupy the La^{3+} site in the lutetium perovskite results in $C \approx 2\text{-}3 \times 10^{-42}$ s^3.

The size and mass of La^{3+} and Lu^{3+} are not so different, therefore the inclusion of an additional ≈5% of oxygen vacancies is needed to reach the experimental value of $C \approx 1\text{-}2 \times 10^{-41}$ s^3 in $LaLuO_3$.

Note that the other Lu-based compound studied in this work, $LuAlO_3$ behaves as expected for a crystalline material (Figure 2(a)). In this case, the much smaller size of Al^{3+} prevents the substitution of Lu^{3+} into the B site of the perovskite $LuAlO_3$.

On the other hand, 5% of RE-ion vacancies results in $C \approx 6 - 7 \times 10^{-41}$ s^3, which are in very good agreement with the values reported in Figure 5(b). In this case, the large mass of the RE-ions dominates completely over the effect of oxygen vacancies.

We have also calculated *ab initio* the energy of A-B atomic substitutions in $LaLuO_3$, $NdScO_3$, and $NdGaO_3$. Our calculations based on the GGA-PBE exchange-correlation potential[52] show that the energy required to exchange those atoms is attainable for the case of La/Lu due to their relatively similar size. In a calculation with 12.5% La/Lu exchanges, the energy required is only about 800 K per lanthanide, whereas it becomes 4 (9) times larger for $NdScO_3$ ($NdGaO_3$). Similar calculations showed that the energy required to introduce a Nd-vacancy is much smaller in $NdScO_3$ compared to $NdGaO_3$.

These results support the idea of an intrinsic number of atomic substitutions and vacancies in $LaLuO_3$ and $REScO_3$, irrespective of the crystal quality and synthetic method.

Finally, looking at Figure 2(d), the thermal conductivity of many $REScO_3$ will be ≈2 W/mK or lower at very high temperatures, similarly to more complex oxides, like YSZ. Along with their high melting point, exceeding 2000 °C, and relatively high thermal expansion coefficient[53] ≈ 8-10 ppm/K, $REScO_3$ could be interesting for applications as crystalline thermal barriers which allow the growth of functional epitaxial oxides on top.

In summary, we have measured the temperature dependence of the thermal conductivity of 27 of the most common single-crystal oxide substrates used for growing epitaxial thin-film oxides. From the analysis of these data we were able to discern between the different relevant contributions to the phonon-relaxation time in different families of oxides.

Particularly interesting is the huge reduction of the thermal conductivity observed in $REScO_3$ perovskites in spite of their high crystalline quality. Our analysis proves that ≈4%-5% of vacancies at the RE-site account for this effect. *Ab initio* calculations suggest that this may be intrinsic to $REScO_3$, irrespective of the method of synthesis.

The information presented in this paper is relevant to design crystalline oxides with a desired thermal conductivity and to select the appropriate substrate for applications in which heat management is important.

See the supplementary material for a complete description of the analysis of the 3ω data. The experimental data of the thermal conductivity for all the samples studied in this work are also available in the supplementary material, as well as the results of the phonon velocity, density and Debye temperature used in each case.

We thank Professor Chang-Beom Eom and Dr. Camilo Gonzalez-Quintela, from the University of Madison, and Professor Darrell Schlom from Cornell University, for discussion and calling our attention to the existence of atomic interdiffusion and vacancies in $REScO_3$. We also thank Dr. Sebastián Reparaz from ICMAB for his assistance during development of the 3ω system. CrysTec GmbH is acknowledged for providing us the single crystal substrates of this study. This work was supported by the European Research Council (Grant No. ERC StG-259082, 2DTHERMS), and MINECO of Spain (Project No. MAT2013-44673-R) and Xunta de Galicia (Project No. EM2013/037). V.P. acknowledges support from the Ramon y Cajal Program (No. RYC-2011-09024) and E.F.V. from Xunta de Galicia through the I2C plan.

[1] *Thermal Conductivity. Theory, Properties, and Applications, Physics of Solids and Liquids*, edited by T. M. Tritt (Kluwer Academic/Plenum Publishers, New York, 2004).
[2] D. T. Morelli and G. A. Slack, in *High Thermal Conductivity Materials*, edited by S. L. Shinde and J. S. Goela (Springer, 2006).
[3] D. G. Schlom, L.-Q. Chen, C. J. Fennie, V. Gopalan, D. A. Muller, X. Pan, R. Ramesh, and R. Uecker, MRS Bull. **39**, 118 (2014).

[4] D. G. Cahill, Rev. Sci. Instrum. **61**, 802 (1990).
[5] J. Álvarez-Quintana and J. Rodriguez-Viejo, Sens. Actuators, A **142**, 232 (2008).
[6] M. Kareev, S. Prosandeev, J. Liu, C. Gan, A. Kareev, J. W. Freeland, M. Xiao, and J. Chakhalian, Appl. Phys. Lett. **93**, 061909 (2008).
[7] G. A. Slack and S. Galginaitis, Phys. Rev. **133**, A253 (1964).
[8] G. A. Slack, Phys. Rev. **105**, 829 (1959).
[9] C. T. Walker and R. O. Pohl, Phys. Rev. **131**, 1433 (1963).
[10] M. R. Winter and D. R. Clarke, Acta Mater. **54**, 5051 (2006).
[11] G. K. White and O. L. Anderson, J. Appl. Phys. **37**, 430 (1966).
[12] Y. A. Chang, J. Phys. Chem. Solids **23**, 697 (1967).
[13] I. Suzuki, I. Ohno, and O. L. Anderson, Am. Mineral. **85**, 304 (2000).
[14] O. L. Anderson, J. Phys. Chem. Solids **24**, 909 (1963).
[15] K. A. Pestka II, E. S. Scott, and Y. Le Page, AIP Adv. **1**, 032154 (2011).
[16] M. Janovska *et al.*, J. Phys.: Condens. Matter **24**, 385404 (2012).
[17] K. A. Pestka, J. D. Maynard, A. Soukiassian, X. X. Xi, D. G. Schlom, Y. Le Page, M. Bernhagen, P. Reiche, and R. Uecker, Appl. Phys. Lett. **92**, 111915 (2008).
[18] D. T. Morelli, J. Mater. Res. **7**, 2492 (1992).
[19] H. H. Barrett, Phys. Lett. A **26**, 217 (1968).
[20] A. Senyshyn *et al.*, J. Phys.: Condens. Matter **17**, 6217 (2005).
[21] H. J. Reichmann and S. D. Jacobsen, Am. Mineral. **91**, 1049 (2006).
[22] A. E. Gleason *et al.*, Geophys. Res. Lett. **38**, L03340, doi:10.1029/2010GL045860 (2011).
[23] A. Chopeles *et al.*, in *Mineral Spectroscopy: A Tribute to Roger G. Burns*, edited by M. D. Dyar, C. McCammon, and M. W. Schaefer (The Geochemical Society Special Publication, 1996), Vol. 5.
[24] L. Jin *et al.*, Solid State Sci. **14**, 106 (2012).
[25] Y. Ding *et al.*, Comput. Mater. Sci. **82**, 202 (2014).
[26] F. Birch, J. Geophys. Research **66**, 2199, doi: 10.1029/JZ066i007p02199 (1961).
[27] M. Guennou, P. Bouvier, G. Garbarino, and J. Kreisel, J. Phys.: Condens. Matter **23**, 395401 (2011).
[28] S. Piskunov, E. Heifets, R. I. Eglitis, and G. Borstel, Comput. Mater. Sci. **29**, 165 (2004).
[29] A. G. Gavriliuk, V. V. Struzhkin, I. S. Lyubutin, M. I. Eremets, I. A. Trojan, and V. V. Artemov, JETP Lett. **83**, 37 (2006).
[30] I. Suzuki, E. Ohtami, and M. Kumazawa, J. Phys. Earth **27**, 53 (1979).
[31] J. M. Ziman, *Electrons and Phonons, International Series of Monographs in Physics* (Clarendon, Oxford, 1963).
[32] I. Inbar and R. E. Cohen, Ferroelectrics **194**, 83 (1997).
[33] K. A. Müller and H. Burkard, Phys. Rev. B **19**, 3593 (1979).
[34] G. A. Samara, J. Phys.: Condens. Matter **15**, R367 (2003).
[35] P. E. Hopkins, C. Adamo, L. Ye, B. D. Huey, S. R. Lee, D. G. Schlom, and J. F. Ihlefeld, App. Phys. Lett. **102**, 121903 (2013).
[36] J. F. Ihlefeld, B. M. Foley, D. A. Scrymgeour, J. R. Michael, B. B. McKenzie, D. L. Medlin, M. Wallace, S. Trolier-McKinstry, and P. E. Hopkins, Nano Letters **15**, 1971 (2015).
[37] Z. Qu, T. D. Sparks, W. Pan, and D. R. Clarke, Acta Mater. **59**, 3841 (2011).
[38] K. Ke, C. Adamo, D. G. Schlom, M. Bernhagen, R. Uecker, and P. Schiffer, Appl. Phys. Lett. **94**, 152503 (2009).
[39] D. Walton, Phys. Rev. B **1**, 1234 (1970).
[40] G. A. Slack, Phys. Rev. **126**, 427 (1962).
[41] G. A. Slack and D. W. Oliver, Phys. Rev. B **4**, 592 (1971).
[42] P. Hohenberg and W. Kohn, Phys. Rev. **136**, B864 (1964).
[43] K. Schwarz and P. Blaha, Comput. Mater. Sci. **28**, 259 (2003).
[44] R. H. Mitchell and R. P. Liferovich, J. Solid State Chem. **177**, 2188 (2004).
[45] J. L. Berdot, H. Gillier-Pandraud, and H. Brusset, Phase Transition **38**, 127 (1992).
[46] A. I. Liechtenstein, V. I. Anisimov, and J. Zaanen, Phys. Rev. B **52**, R5467 (1995).
[47] R. Uecker, B. Velickova, D. Klimma, R. Bertrama, M. Bernhagena, M. Rabea, M. Albrechta, R. Fornaria, and D. G. Schlom, J. Cryst. Growth **310**, 2649 (2008).
[48] R. Uecker, D. Klimm, R. Bertram, M. Bernhagen, I. Schulze-Jonack, M. Brützam, A. Kwasniewski, Th.M. Gesing, and D. G. Schlom, Acta Phys. Pol. A **124**, 295 (2013).
[49] B. Velickov, V. Kahlenberg, R. Bertram, and M. Bernhagen, Z. Kristallogr. **222**, 466 (2007).
[50] R. Uecker, R. Bertram, M. Brutzam, Z. Galazka, T. M. Gesing, C. Guguschev, D. Klimm, M. Klupsch, A. Kwasniewski, and D. G. Schlom, "Large-lattice-parameter perovskite single-crystal substrates," J. Cryst. Growth (published online, 2016).
[51] K. L. Ovanesyan, A. G. Petrosyan, G. O. Shirinyan, C. Pedrini, and L. Zhang, J. Cryst. Growth **198-199**, 497 (1999).
[52] J. P. Perdew, K. Burke, and M. Ernzerhof, Phys. Rev. Lett. **77**, 3865 (1996).
[53] M. D. Biegalski, J. H. Haeni, S. Trolier-McKinstry, D. G. Schlom, C. D. Brandle, and A. J. Ven Graitis, J. Mater. Res. **20**, 952 (2005).